PERSPECTIVE • OPEN ACCESS

Internal biogas reforming in solid oxide and proton conducting fuel cells: progress, challenges and perspectives

Journal of Physics: Energy

PERSPECTIVE

Internal biogas reforming in solid oxide and proton conducting fuel cells: progress, challenges and perspectives

Stephanie E Wolf[1,2], Jan Uecker[1,2], Niklas Eyckeler[1,2], Leon Schley[1,2], L G J (Bert) de Haart[1], Vaibhav Vibhu[1,*] and Rüdiger-A Eichel[1,2]

[1] Institute of Energy Technologies, Fundamental Electrochemistry (IET-1), Forschungszentrum Jülich GmbH, 52425 Jülich, Germany
[2] Institute of Physical Chemistry, RWTH Aachen University, 52074 Aachen, Germany
[*] Author to whom any correspondence should be addressed.

E-mail: v.vibhu@fz-juelich.de

Keywords: biogas reforming, solid oxide fuel cell (SOFC), solid proton conducting fuel cell (SPCFC), syngas, degradation

OPEN ACCESS

RECEIVED
10 December 2024

REVISED
13 February 2025

ACCEPTED FOR PUBLICATION
26 February 2025

PUBLISHED
14 March 2025

Abstract

The internal reforming of biogas, a mixture containing carbon dioxide (CO_2) and methane (CH_4), in solid oxide and solid proton conducting fuel cells (SOFCs, SPCFCs) is a sustainable and efficient method to produce syngas ($H_2 + CO$) in combination with highly efficient electrical power generation. Reforming processes convert biogas into syngas by steam reforming, dry reforming, or partial oxidation, which then undergoes electrochemical reactions in the SOFCs/SPCFCs to produce electricity and heat. The dry methane reforming process of the anthropogenic greenhouse gases CH_4 and CO_2 into biogas can result in co-generation of electrical power and syngas mixtures of CO:H_2 relevant for large-scale industrial processes like the Fischer–Tropsch process. Herein, a short review of promising developments in the literature concerning the internal dry reforming of biogas (CH_4 and CO_2) in oxygen-ion conducting and proton-conducting fuel cells is provided. The thermodynamics of different reforming processes, the advantages, disadvantages, and the fundamental electrochemical processes in SOFCs and SPCFCs are discussed comprehensively and comparatively. In addition, this article aims to provide a perspective on current gaps and possible future research efforts.

1. Introduction

Hydrogen (H_2) is a promising alternative to fossil fuels due to its high calorific value, high energy density, and naturally abundant occurrence. It can be stored by compression or liquefaction as a fuel for later use in combustion engines or turbines in the transportation sector [1]. The chemical industry used 53 Mt of H_2 in 2022 as a sustainable feedstock to produce essential platform chemicals such as ammonia (60%), methanol (30%), and synthetic fuels. Ten percent of hydrogen was used as a reducing agent in steel and iron sectors as well as for the processing of cement, ceramics, aluminum, and copper [2]. The varied production pathways of hydrogen include technologies such as unabated coal gasification (21%) and as a byproduct of the petrochemical naphtha reforming process (16%). The primary source of large-scale hydrogen production in 2022 was methane steam reforming (MSR), which accounted for 62% of the global hydrogen production. MSR is a mature and commercially established process operated between 700 °C and 1000 °C at 15–50 bar, during which methane reacts endothermically with steam to produce hydrogen and carbon monoxide in the ratio 3:1 as given in equation (1). This gas mixture of CO and H_2 is referred to as syngas and the carbon monoxide reacts in the second process step in the exothermic equilibrium water–gas shift (WGS) reaction with steam to carbon dioxide (equation (2)) [3]. The reaction equilibrium can be driven to the WGS products by adding steam to the gas stream at the inlet of the shift reactor to obtain the desired product ratios,

$$CH_{4(g)} + H_2O_{(g)} \rightarrow 3H_{2(g)} + CO_{(g)} \qquad \Delta H_{800\,^\circ C} = +206\,\mathrm{kJ\cdot mol^{-1}} \tag{1}$$

$$CO_{(g)} + H_2O_{(g)} \leftrightharpoons CO_{2(g)} + H_{2(g)} \qquad \Delta H_{800\,^\circ C} = -41\,\mathrm{kJ\cdot mol^{-1}} \tag{2}$$

Table 1. Typical components of landfill biogas and natural gas. Reprinted from [6], Copyright (2014), with permission from Elsevier.

Component	Unit	Natural gas	Landfill biogas
CH_4	vol%	81–89	30–65
CO_2	vol%	0.67–1	25–47
N_2	vol%	0.28–14	<1–17
O_2	vol%	0	<1–3
H_2	vol%	NA	0–3
Higher hydrocarbons	vol%	3.5–9.4	NA
H_2S, NH_3	ppm	NA	0–500
Total chlorines	$mg{\cdot}Nm^{-3}$	NA	0.3–225
Siloxane	$mg{\cdot}g\text{-}dry^{-1}$	NA	<0.3–36

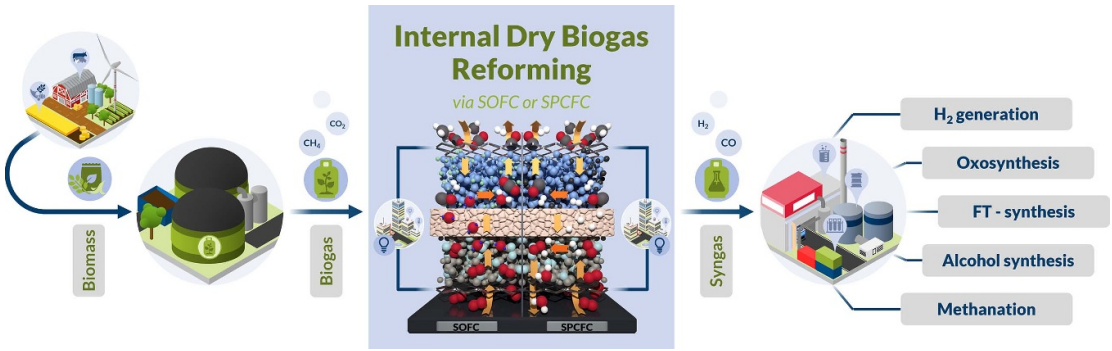

Figure 1. Schematic process scheme for the biogas utilization in an SOFC system integrated into the value chain.

The partial oxidation of methane is an exothermic reaction given in equation (3) can be combined with MSR to increase the thermal conversion efficiency of H_2 and is subsequently called auto-thermal reforming,

$$CH_{4(g)} + \frac{1}{2}O_{2(g)} \rightarrow 2H_{2(g)} + CO_{(g)} \qquad \Delta H_{800\,^\circ C} = -38\ \mathrm{kJ \cdot mol^{-1}} \tag{3}$$

Using natural and renewable resources, such as biogas from biomass, could lead to carbon dioxide (CO_2)-negative syngas mixtures and thus green hydrogen production. The biomass may be converted to biogas via biological degradation, which gives a product gas mixture composed of methane (CH_4), carbon dioxide (CO_2), nitrogen (N_2), oxygen (O_2), and H_2, as well as traces of ammonia (NH_3), higher order hydrocarbons (C_xH_{2x+2}), e.g. ethane (C_2H_6), and contaminants such as sulfur, chlorides, and siloxanes depending on the production process (table 1) [4–6]. The subsequent catalytic reforming process gives the gaseous product syngas and high-purity H_2. Carrying out the reforming process in a fuel cell system enables the subsequent conversion of H_2 and CO to H_2O and CO_2, thereby generating electrical power. Combining this highly flexible and efficient power generation process with the production of valuable gaseous intermediates, such as CO and H_2, increases the system's efficiency. Remaining product gases can be used, for example, in the Fischer–Tropsch synthesis to produce ethanol or liquid hydrocarbons to be used as synthetic fuels [7]. A schematic example of a process scheme containing the listed applications above is shown in figure 1.

The dry methane reforming process (DMR) has gathered increased interest in the last years due to the possibility of simultaneously converting the anthropogenic greenhouse gases CH_4 and CO_2 into valuable syngas mixtures of CO:H_2 in the 1:1 ratio relevant for the large-scale industrial Fischer–Tropsch process and the downstream processes such as the oxo-synthesis of alcohols and aldehydes (equation (4)) [8]. The CO_2 contained in the biogas does not have to be separated in an elaborate process from the CH_4 to be processed [9],

$$CH_{4(g)} + CO_{2(g)} \rightarrow 2H_{2(g)} + 2CO_{(g)} \qquad \Delta H_{800\,^\circ C} = +247\ \mathrm{kJ \cdot mol^{-1}} \tag{4}$$

As CO_2 is a thermodynamically stable oxidizing agent, its use in the DMR leads to a highly endothermic reaction that necessitates higher reaction temperatures than steam reforming or partial methane oxidation. The endothermic and reversible reforming reaction of CH_4, as given in equation (4), starts around 350 °C with the selectivity favoring the formation of steam and carbon as shown in figure 2 [10].

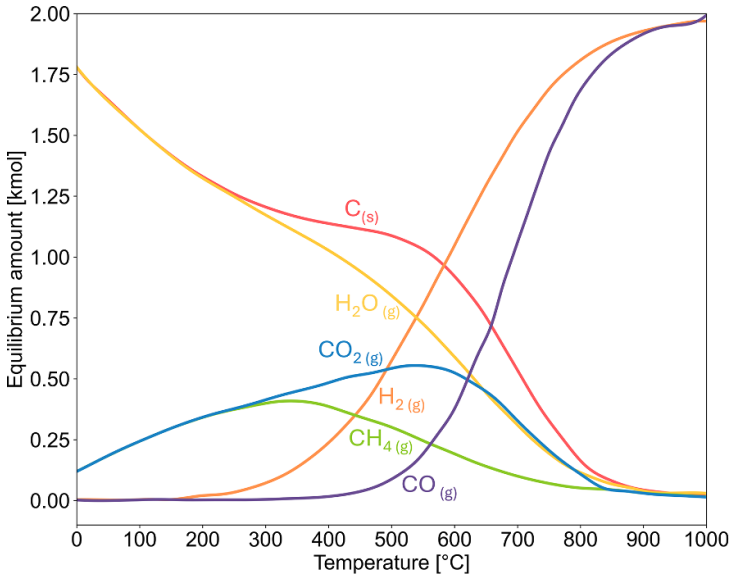

Figure 2. Thermodynamic equilibrium calculated for the composition of 1 kmol of CH_4 and CO_2 at 1 atm by HSC Chemistry 7.1. Reprinted from [10], Copyright (2013), with permission from Elsevier.

With increased operating temperature, the selectivity shifts toward the formation of syngas and is mostly favored above 727 °C. The reverse water gas shift reaction (RWGS) additionally shifts the syngas selectivity to $H_2/CO < 1$ and increases the unavoidable formation of the side product steam between 400 °C and 820 °C [11].

Among other side reactions, the reactions that produce carbon are given by equations (5)–(8), and include the decomposition of CH_4, which dissociates completely to form carbon on the catalyst surface, thereby producing H_2 and taking place above 557 °C (equation (7)). The Boudouard reaction is known to occur below 700 °C and describes the CO disproportionation reaction to CO_2 and surface carbon. With increased temperatures, the thermodynamic formation of carbon becomes less favored until almost no carbon is observed at around 900 °C [12, 13]. These side reactions necessitate high operating temperatures for the dry reforming of methane (DRM) above 820 °C, to enhance the syngas reaction selectivity while minimizing the impact of the RWGS steam formation [10, 12, 13] and to avoid the range for maximum carbon deposition reported (557 °C–700 °C). The magnitude of side reactions can be influenced by selecting the optimal reaction temperature, the feed gas ratio, and operating pressure [13, 14],

Hydrogenation

$$CO_{2(g)} + 2H_{2(g)} \rightleftharpoons C_{(s)} + 2H_2O_{(g)} \qquad \Delta H_{800^\circ C} = -134\,\mathrm{kJ}\cdot\mathrm{mol}^{-1} \tag{5}$$

$$CO_{(g)} + H_{2(g)} \rightleftharpoons C_{(s)} + H_2O_{(g)} \qquad \Delta H_{800^\circ C} = -175\,\mathrm{kJ}\cdot\mathrm{mol}^{-1} \tag{6}$$

Decomposition

$$CH_{4(g)} \rightleftharpoons C_{(s)} + 2H_{2(g)} \qquad \Delta H_{800^\circ C} = +75\,\mathrm{kJ}\cdot\mathrm{mol}^{-1} \tag{7}$$

Disproportionation

$$2CO_{(g)} \rightleftharpoons C_{(s)} + CO_{2(g)} \qquad \Delta H_{800^\circ C} = -172\,\mathrm{kJ}\cdot\mathrm{mol}^{-1} \tag{8}$$

The DMR process is not considered a mature and fully developed industrial process yet, regardless of the evident economic and environmental advantages of reprocessing CH_4 and CO_2 to produce syngas. High operating temperatures are required to avoid thermodynamically favored side reactions, and the catalysts under consideration must withstand thermal sintering and subsequent catalyst deactivation [15–18]. Noble metal catalysts such as Ru, Rh, Ir, Pt, and Pd have been investigated intensively due to their known catalytic activity in heterogeneous chemistry reactions and high carbon deposition resistivity [19, 20]. However, the prevalent use in scale-up applications is limited due to high investment costs. Thus, the transition metals Ni and Co have been considered for their high coke-formation resistance and catalytic activity [21]. To address the challenges of stability and catalytic activity, several design strategies have been employed. Bimetallic noble-metal–Ni catalysts have been tested to increase the Ni particles dispersion and avoid agglomeration [22–25]. The performance and robustness of transition metal catalysts, e.g. Ni, have been modified by employing support oxides such as rare earth oxides, Al_2O_3, CeO_2, YSZ (8 mol%Y_2O_3–ZrO_2), Nb_2O_5, TiO_2,

ZrO_2, La_2O_3, Y_2O_3, as well as combined versions [26]. The support oxides' highly mobile lattice oxygen ions (O^{2-}) and their surface vacancies led to bifunctional reaction pathways, which enhanced the catalytic performance and had beneficial effects on long-term stability.

Despite significant progress regarding catalyst design, developing highly efficient catalysts with high activity and long-term stability remains a considerable challenge. Moreover, the high energy demand for the endothermic reforming reaction has to be considered when integrating the process into existing industrial facilities. The utilization of internal biogas reforming in fuel cells is an efficient and economical direct way to convert chemical energy in the form of fuels into electrical power, bypassing the Carnot limitations [27].

2. Solid oxide fuel cells (SOFCs)

SOFCs are gaining increased interest due to their rapidly growing entry into the commercial market. These ceramic oxide-based cells convert hydrocarbon-containing fuels into electrical power or syngas, depending on the operating conditions [28–30]. High fuel flexibility enables the utilization of biogas, natural gas, as well as gas streams containing CH_4, CO_2, CO, H_2, and H_2O. During the reaction technical efficiencies of up to 100% can be achieved due to favorable thermodynamics and reaction kinetics at operating temperatures between 650 °C and 900 °C [7]. The high operating temperatures are ideal for DMR utilizing captured CO_2 to produce syngas from biogas (carbon capture utilization) and generate electrical power [31–33].

A schematic illustration of the working principles is depicted in figure 3 for the use of H_2/H_2O and CH_4/CO_2 input feeds, respectively. The cell is composed of two porous ionic–electronic-conducting electrodes and an ionic conducting electrolyte in between. At the air electrode, the oxygen molecules are reduced to oxygen ions, which then migrate through the electrolyte to the fuel electrode,

$$\frac{1}{2}O_{2(g)} + e^- \rightarrow O^{2-} \tag{9}$$

At the fuel electrode during the direct internal reforming of biogas (CH_4 and CO_2), the CO_2 acts as an oxidizing agent. The oxidation of CH_4 is based on several possible dissociation and oxidation steps according to the methane combustion mechanism, forming radicals, which result in the formation of CO and H_2 [34]. There are several ways to form H_2 and CO and possible reaction pathways are described in the following equations.

According to equation (10), CH_4 can react with an impact partner M′ to give the radicals CH_3° and H°.

$$CH_{4(g)} + M' \rightarrow CH_3^\circ + H^\circ \tag{10}$$

The dissociation of CO_2 can result in CO and an oxide radical O° (equation (11)). Another possibility is the reaction of CO_2 with the H° radical, which results in the formation of steam and an oxide radical (equations (12) and (13)),

$$CO_{2(g)} \rightarrow CO_{(g)} + O^\circ \tag{11}$$
$$CO_{2(g)} + H^\circ \rightarrow CO_{(g)} + OH^\circ \tag{12}$$
$$OH^\circ + OH^\circ \rightarrow H_2O_{(g)} + O^\circ \tag{13}$$

The oxide radical oxidizes the CH_3° radical and initiates the conversion to CO and H_2.

$$CH_3^\circ + O^\circ \rightarrow CH_2O_{(g)} + H^\circ \tag{14}$$
$$CH_2O_{(g)} + H^\circ \rightarrow CHO^\circ + H_{2(g)} \tag{15}$$
$$CHO^\circ + H^\circ \rightarrow CO_{(g)} + H_{2(g)} \tag{16}$$

The fuel gas stream in the SOFC operated with a feed gas of CH_4 and CO_2 contains therefore H_2 and CO. The O^{2-} ions that previously migrated from the air to the fuel electrode side, now react in an exothermic oxidation reaction with H_2 and CO, as shown in figure 3, to give steam (H_2O) and CO_2 as the end-products. During these oxidation reactions, electric current is released in the form of electrons. The generated electrical power can be subsequently used in the electrification of sectors such as mobility, residential heating and cooling, as well as industrial production,

$$H_{2(g)} + O^{2-} \rightarrow H_2O_{(g)} + 2e^- \tag{17}$$
$$CO_{(g)} + O^{2-} \rightarrow CO_{2(g)} + 2e^- \tag{18}$$

In methane reforming, Ni-based materials are widely used catalysts, which play a critical role in facilitating the conversion of methane to syngas. Their prevalent role also extends to SOFCs, where

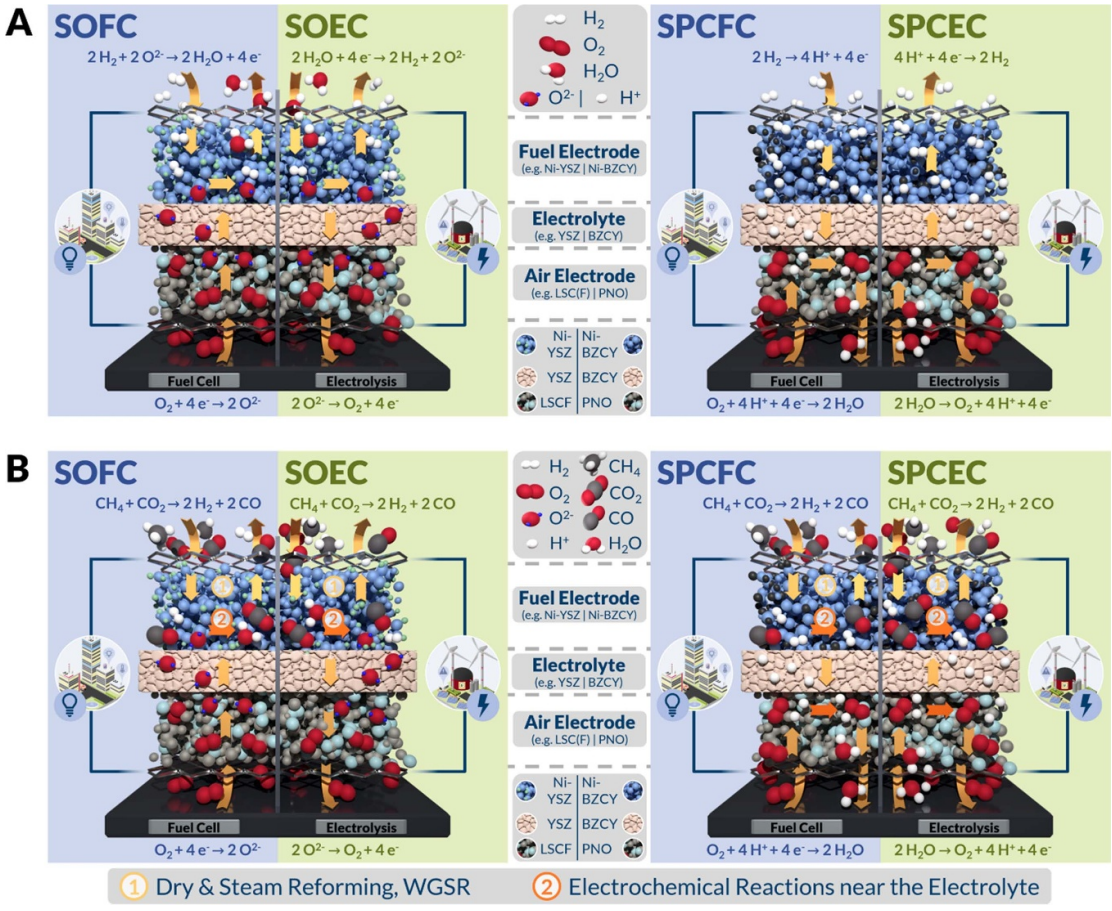

Figure 3. Schematic comparison of the functional principles in solid oxide and solid proton-conducting cells, showing the electrochemical reactions in fuel cell (SOFC, SPCFC) and electrolysis (SOEC, SPCEC) mode for (A) operation in H_2/H_2O and (B) CH_4/CO_2 input gas streams.

Ni-cermets (ceramic metals) are valued as electrodes for fuel conversion due to their high catalytic activity and excellent electronic conductivity. Ni-8YSZ (8 mol% yttria-stabilized zirconia) and Ni-GDC (gadolinium-doped ceria, $Ce_{0.8}Gd_{0.2}O_{1.9}$) are the most commonly employed fuel electrode materials in solid oxide cells (SOCs). While YSZ and GDC exhibit high ionic conductivity, Ni grants high electronic conductivity to the composite electrode materials. At the triple-phase boundary (TPB), the fuel gas reacts with the O^{2-} migrating from the air electrode to produce electronic power. Currently, mixed ionic and electronic conducting cobalt-based lanthanum strontium perovskites such as $La_{0.6}Sr_{0.4}CoO_{3-\delta}$ and $La_{0.6}Sr_{0.4}Co_{0.2}Fe_{0.8}O_{3-\delta}$ (LSC(F)) are used for the oxygen reduction reaction due to their advantageous oxygen diffusion properties and electronic (σ_e) and ionic (σ_i) conductivities in air as well as their higher oxygen permeability [35]. In addition to their use as fuel cells, high-temperature SOCs can also be operated in reverse as solid oxide electrolysis cells (SOECs) or in a mixed mode [3]. When operating as an SOEC, the electrochemical reactions are reversed: fuel gases are reduced at the Ni-cermet electrode, and oxygen is produced at the air electrode. This process allows the conversion of electrical power to syngas from gas mixtures containing various gaseous reactants, e.g. H_2O, H_2, CH_4, CO, and CO_2. When operated as an SOEC with CH_4/CO_2 gas input streams, the internal reforming reaction leads to an operating feed gas mixture of mainly H_2 and CO identical to the SOFC operation. However, the operation in SOEC mode allows the tailoring of the syngas produced from the system by reducing the remaining CO_2 to CO as shown in figure 3.

Several reviews have been written in detail on the employed state-of-the-art fuel and air electrode materials [36, 37], their fabrication methods [38, 39], as well as the ongoing material development research [3, 40, 41]. Therefore, the authors will not go into more detail.

Current research regarding the internal dry reforming of CH_4 and CO_2 is investigated on a cell level to demonstrate the mechanical feasibility and optimize the parameters impacting fuel conversion selectivity and reaction rate. The operating parameters examined include temperature, gas composition, and current density. An increase in temperature has been shown to lead to a higher conversion efficiency of CH_4 in dry-reforming [42]. This is based on the thermodynamics of the endothermic reaction and the higher chance

of carbon removal at elevated operating temperatures (figure 2). Both experimental and theoretical investigations on the catalytic properties of Ni-YSZ fuel electrodes have shown that conversion of CH_4/CO_2 starts at around 450 °C. Up to 620 °C, the dry reforming and the RWGS reaction ensure the syngas production, whereby the CO production is steeper than for H_2. Above 620 °C, the relative CH_4 conversion reaches around 90%. In this temperature region, the conversion to CO increases continuously, while the concentration of H_2 decreases slightly. The effect of current density on the DRM reaction shows a similar trend. With increasing current density and thus increasing the number of electrons, the electrochemical activity of the catalyst and the conversion rate increase irrespective of temperature and feed gas composition [42].

An in-depth investigation of the CH_4/CO_2 ratio on the dry reforming reaction showed increasing conversion efficiency with decreasing partial pressures of CH_4. For a feed gas ratio of $CH_4/CO_2 = 1.5$, an efficiency of around 17% percent was observed. This increased to 22% when switching to a ratio of $CH_4/CO_2 = 0.5$. This trend was attributed to the gas distribution and the increase of unwanted side reactions of CH_4 at high pCH_4 as well as catalyst saturation. Low feed gas ratios of CH_4/CO_2, on the other hand, with an increased partial pressure of the oxidant CO_2 shift the reaction equilibrium to the formation of syngas [43–46]. Nevertheless, a positive impact of the CH_4/CO_2 ratio was observed for the DRM reaction rate with a maximum around $R_{CH4/CO2} = 1.5$, which was attributed to the adsorption competition of CH_4 and CO_2 at the catalyst surface [42]. Several researchers suggested a ratio of 1:1 for CH_4 and CO_2 as the optimal feed gas composition [42, 47]. An in-depth study of electrical power production and its dependence on the methane content in biogas has shown that the maximum power production occurs at 45% methane. This corresponds to the maximum production of H_2 and CO by internal dry reforming [48].

The direct use of CH_4 in an SOFC has been extensively studied and various systems have been proposed. The behavior of planar SOFCs supplied with simulated biogas compositions, namely bio-hydrogen (bio-H_2) and bio-CH_4, from anaerobic digestion was investigated [49]. The internal reforming reaction was stable under the current load of 0.5 A·cm^{-2} for the anode-supported cell and 0.3 A·cm^{-2} for the electrolyte-supported cell at 800 °C for 50 h. The evaluation of three configurations combining biogas-fueled SOFC micro Combined Heat and Power (micro-CHP) systems for residential applications included anode gas recirculation, steam reforming, and partial oxidation [50]. The study included the analysis of cell operating voltage, fuel utilization, CHP efficiency, biogas fuel composition, and excess air for stack temperature control. The results showed that these systems have significant potential to generate additional electricity, particularly if the partial oxidation system is integrated with other power generation equipment and optimized accordingly. Experimental and theoretical approaches were employed to investigate the direct dry-reforming of biogas and with CO_2 -lean to CO_2 -rich conditions on Ni-based SOFC anodes [51]. Reforming kinetics were incorporated into the model to predict the gas composition profile along the fuel channel. The model was validated using experimentally derived polarization curves. The co-generation of electricity and syngas from methane was investigated by incorporating dendrite pore channels in the Ni/CeO_2-Al_2O_3 catalyst, thereby increasing the performance by 25% to 1.04 W·cm^{-2} at 800 °C with 25% CH_4/Ar fuel gas [52].

In addition to the advantageous fuel flexibility, SOFCs exhibit easy cell stack manufacturability without the disadvantage of operating with corrosive liquids as used in low-temperature proton exchange-membrane fuel cells. Nevertheless, high operating temperatures above 650 °C are detrimental to the cell materials and other essential system components such as interconnects, sealants, and coatings. Hence, scientific research is attempting to lower the fuel cell operating temperature below 700 °C. As this drastically increases the resistivity of the electrodes and the electrolyte, due to the hindered ion conducting mechanism and the drastically handicapped thermally activated processes, new materials have to be considered to address the future challenges of SOFCs [53]. One strategy to lower the operating temperature is to switch the material class from oxygen ion-conducting ceramics to proton-conducting materials.

In summary, SOFCs operated above 650 °C are currently being investigated for the internal dry reforming of biogas using experimental and theoretical approaches mostly on a cell level to demonstrate feasibility and optimize parameters such as temperature, gas composition, and current density for high fuel conversion, product selectivity, and an optimized reaction rate. Ni-based materials are widely used catalysts, which play a critical role in facilitating the conversion of methane to syngas. Different modeling approaches for SOFC systems have been employed to assess the potential for electricity generation and to investigate different gas composition profiles.

3. Proton conducting ceramic cells

Solid proton conducting fuel cells (SPCFCs) are based on proton-conducting electrolytes and electrode materials that enable high cell efficiencies at intermediate operating temperatures of 400 °C–650 °C due to

faster proton conduction and lower activation energy for bulk proton transfer (0.3–0.5 eV) compared to oxygen ion conduction (0.8–0.9 eV) [54, 55]. The charge carriers in the typical Y-doped $BaZrO_3$–$BaCeO_3$ materials [56], i.e. $BaZr_{1-x-y}Ce_xY_yO_{3-\delta}$ (BZCY), are protons, electron holes, and oxygen ions depending on the material composition, the operating temperature, and the gas atmosphere. Promising electrolyte materials include $BaCe_{0.7}Zr_{0.1}Y_{0.1}Yb_{0.1}O_{3-\delta}$ (BCZYYb7111) [57] and $BaCe_{0.4}Zr_{0.4}Y_{0.1}Yb_{0.1}O_{3-\delta}$ (BCZYYb4411) [58]. The high ceria content facilitates high proton conductivity and good sinterability based on the relatively high basicity of ceria compared to zirconia. In contrast, high levels of zirconia result in greater chemical stability in steam-containing gas streams due to the relatively high acidity [55, 59]. Several promising candidates have been identified as air electrode materials, including $BaCo_{0.4}Fe_{0.4}Zr_{0.1}Y_{0.1}O_{3-\delta}$ (BCFZY) [57], $PrBa_{0.5}Sr_{0.5}Co_{1.5}Fe_{0.5}O_{6-\delta}$ (PBSCF) [60], $Ba_{0.5}Sr_{0.5}Co_{0.8}Fe_{0.2}O_{3-\delta}$ (BSCF) [61] or $Pr_2NiO_{4+\delta}$ (PNO) [55]. Ni-based cermets are considered for the fuel electrode, combining the Ni metal particles with a proton-conducting electrolyte material as seen in SOFCs [62].

Electron holes are formed by oxygen incorporation in the perovskite lattice given by the endothermal reaction in equation (19). The electron–hole prevalence causes electron leakages through the electrolyte layer and lowers the faradaic efficiency compared to high-temperature SOFCs. With increased operating temperature, the electron–hole formation is enhanced, however, predominantly observed in electrolysis mode and minimal for SPCFCs [63, 64].

$$\frac{1}{2}O_{2(g)} + V_O^{\cdot\cdot} \leftrightharpoons O_O^x + 2h^{\cdot} \tag{19}$$

Protonic conductivity is enhanced by B-site doping with suitable trivalent elements such as Y, Nd, Sm, Yb, or Gd. This leads to the formation of oxygen-ion vacancies, which play a crucial role in the formation of mobile protons. In SPCFCs, as shown in figure 3, hydrogen is supplied to the fuel electrode and dissociates into protons (H^+) and electrons (e^-) (equation (13)). A covalent bond is formed between the lattice oxygen and the proton, thereby enabling thermally activated proton migration through the electrolyte to the air electrode. There, the protons react with oxygen ions to form steam (equation (14)),

$$H_{2(g)} \rightarrow 2H^+ + 2e^- \tag{20}$$

$$\frac{1}{2}O_{2(g)} + 2H^+ + 2e^- \rightarrow H_2O_{(g)} \tag{21}$$

In contrast to SOFCs, SPCFCs use dry fuel gas, which reduces the metal substrate corrosion caused by the relatively high steam concentrations in SOFCs. This difference can improve the long-term stability of metal-supported SPCFCs, for example, and reduce the dependence on critical raw materials [65]. Characteristically, steam is produced in SPCFCs at the cathode, air electrode side, which leaves the products on the fuel electrode side undiluted.

Research into direct methane conversion in SPCFCs has been focused on the use of humidified methane [66–68]. However, recent studies have shown promising results with dry methane using button cells [69, 70]. An emphasis is placed on improving Ni-cermet anode materials to increase catalytic activity and reduce electrode poisoning and/or fouling, e.g. carbon deposition. To improve the catalytic properties of the anode, self-assembled Ni-based bimetallic catalysts doped with small amounts of noble metals, such as Rh, Ru, and Pd, have been proposed [71–74]. This strategy has facilitated high-performing electrode development with improved stability and carbon deposition resistance. Further strategies to mitigate carbon deposition are functionally graded anodes to suppress the cracking reaction [75] and the addition of an on-cell reforming catalyst layer to reduce the exposure of the Ni-cermet to gaseous reactants like CH_4 [69]. An example is the Ni–Cu/Ni–Fe alloys (NCF)-$BaZr_{0.1}Ce_{0.7}Y_{0.1}Yb_{0.1}O_{3-\delta}$ (BZCYYb) cermet layer on a conventional Ni-YSZ anode, which was added to suppress carbon deposition during the short-term testing [76]. The catalytically active NCF alloy was formed by reducing the $Ni_{0.5}Cu_{0.5}Fe_2O_4$ (NCFO) spinel. The BZCYYb backbone in the NCF-BZCYYb layer has been added for increased adsorption of H_2O and CO_2 [77, 78].

The widely employed proton-conducting Y-doped $BaCeO_3$ electrolyte has shown low chemical stability in the CO_2 atmosphere. Doped barium cerates with dopants such as Ti [79], Nb [80], and Zr [81] have been investigated, to improve stability with varied results for the chemical stability and accompanied by decreased proton conductivity [81]. The Zr-doped $BaCeO_3$ has shown the best concession of chemical stability and proton conductivity [82, 83]. To achieve the future goal of commercialized internal DRM in SPCFCs, electrode development must be advanced, and cells at a bench scale will have to be manufactured and tested.

In summary, due to their fast proton conductivity, SPCFCs are operated at intermediate temperatures of 400 °C–650 °C, thereby avoiding the high operating temperatures employed in SOFC testing, which are detrimental to the cell and system materials. Additionally, steam is produced at the cathode, air electrode side, leaving the products on the fuel electrode side undiluted. Recent studies have mainly focused on

improving the currently in-use Ni-based fuel electrode materials to overcome the limited catalytic activity, mitigate carbon deposition, and further increase the sulfur tolerance of SPCFCs. However, the validation of stability is mostly tested for less than 500 h.

4. Challenges and strategies

4.1. Microstructural degradation

The electrochemical reactions previously described for SOFCs and SPCFCs involved the transportation of charge carriers through the conductive materials, e.g. electrons e^- via the metallic Ni, and oxide ion O^{2-} transported via the YSZ matrix in the case of SOFCs. Severe microstructural changes of Ni-cermet fuel electrodes in high-temperature SOFC and SOEC operations have been observed and related to performance degradation in humidified and dry conditions. These Ni-YSZ fuel electrode degradation phenomena cause the loss of electrochemically active TPB sites through particle coarsening and agglomeration of the Ni particles, Ni migration, and reoxidation as shown in figure 4. The main factors facilitating these phenomena include high operating temperatures, the gas composition, e.g. high humidity/steam partial pressure, and applied polarization.

4.1.1. Ni agglomeration

The initial Ni-YSZ microstructure exhibits homogeneous distributed Ni particle distribution. During operation, the average Ni particle size increases and the number of particles decreases. These changes in the local Ni concentration have been attributed to an Ostwald ripening process driven by the surface energy difference between smaller and larger Ni particles [3]. Aimed at minimizing the surface free energy, this process results in larger particles growing at the expense of smaller ones via surface or gas phase diffusion, which leads to microstructural coarsening. Furthermore, the Ni particle percolation loss results in the reduction of electrochemically active TPB sites. Studies on internal methane reforming in SOFC have suggested that the steam content plays a significant role in the coarsening of Ni particles. The investigation of different H_2O:CH_4 ratios on Ni nanoparticles in powdered Ni-GDC cermet anodes has shown that the sinter-probability increases under steam-rich conditions [84]. This phenomenon has also been observed at intermediate operating temperatures around 600 °C, at which the total cell resistance increased from 0.96 to 1.25 $\Omega{\cdot}cm^2$ after 100 h in 67% H_2O/33% CH_4 due to Ni particle agglomeration and reduced electrode porosity [85]. However, anode-supported SOFCs with an Ni-8YSZ anode have also been reported to exhibit aggregation and coarsening of Ni particles for dry gas CH_4:CO_2 mixtures with a ratio $R < 1$ [86]. Nevertheless, although the agglomeration or coarsening of Ni particles has been observed at high temperatures and/or high humidity, independent of polarization, the agglomeration is more severe in electrolysis mode [3, 87].

4.1.2. Ni migration

Independent of the polarization, Ni migration away from the electrolyte has been observed for Ni-YSZ electrodes. One hypothesis describes the loss of electrochemical Ni–Ni contact, Ni coarsening, as the cause of Ni migration. At high temperatures in steam containing atmosphere, gaseous $Ni(OH)_x$ species may migrate away from the electrolyte to places where the Ni^{x+} will be reduced to Ni metal. The Ni particle depletion near the electrolyte results in poor connectivity between the electrolyte and the fuel electrode, which leads to increased ohmic and polarization resistance. Ni migration is not limited to $Ni(OH)_x$, since it occurs in dry CO_2/CO conditions as well [88]. Ni/YSZ cermet anode post-test observations suggested Ni depletion after 1000 h dry methane operation at 950 °C and a constant current density of 400 $mA{\cdot}cm^{-2}$ [89]. Several hypotheses on the Ni migration mechanism for SOCs are currently being discussed [90–93]. Nevertheless, the authors agree that the Ni migration, like the Ni agglomeration, is more severe in electrolysis mode or in an atmosphere with a high steam content. Mogensen *et al* [90] formulated the hypothesis that the Ni migration is an electrical potential facilitated mechanism in reversible SOC fuel electrodes taking place through the surface and/or gas phase transportation of NiOH or $Ni(OH)_2$ dependent on the reaction conditions such as strongly positive or negative polarization and as a result of prior significant Ni–Ni contact loss observed during Ni particle coarsening. As a fundamental consequence, the active TPB region at the still electrically connected Ni particles moves further away from the dense YSZ electrolyte. An alternative hypothesis by Jiao *et al* [93, 94] suggests that changes in the Ni contact angle cause local wettability. With increasing humidity and decreasing contact angle, the authors observed Ni diffusion in SOFC.

4.1.3. Ni reoxidation

High partial pressures of H_2O and/or CO_2 as well as accumulated O^{2-} ions at the TPB may cause Ni to reoxidize to NiO [95]. This reaction coincides with material re-expansion and subsequent mechanical cell

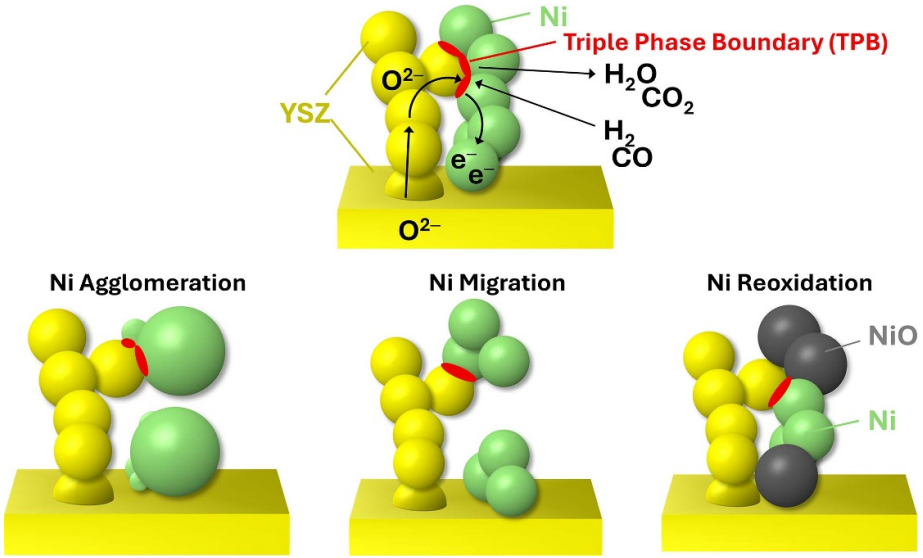

Figure 4. Microstructural changes observed for high-temperature Ni-YSZ fuel electrodes in SOCs.

damage, e.g. cracking and delamination of the SOFC fuel electrode, resulting ultimately in cell failure. Therefore, to mitigate Ni reoxidation, the feed gas ratio of CH_4 to CO_2 has to be controlled [47, 85, 96].

4.2. Catalyst deactivation

The loss of catalyst activity is termed deactivation and occurs due to physical and chemical processes over time. In addition to the discussed microstructural changes that are dependent on operation temperature and gas composition, the main causes of deactivation include poisoning and coking/fouling of the electrode in the DMR, which will be discussed in more detail in this chapter.

4.2.1. Carbon deposition

Carbon deposition and coking are challenges in SOFC or SOEC systems when using a hydrocarbon-containing gas feedstock. Under direct DMR conditions, carbon deposition can take place due to the decomposition of methane (equation (7)), the Boudouard reaction (equation (8)), and nickel-catalyzed reactions [95, 97]. Carbon deposition is critical to the long-term stability of an SOFC system as it can cause detrimental microstructural changes at the cell level. One consequence is mechanical stress, which is induced as solid carbon forms in the Ni-YSZ fuel electrode. This can lead to fractures in the microstructure and break the network connectivity leading to rapid and irreversible degradation [95, 98]. Another issue is the deactivation of active sites in the Ni-YSZ fuel electrode by a decrease in TPB length. Here carbon is blocking the TPBs and hindering the electrochemical reaction leading to lower performances [97]. Furthermore, the nickel coarsening in the Ni-YSZ fuel electrode can be accelerated by coking leading to an accelerated degradation [99].

The operating conditions of an SOFC system are majorly influencing the carbon deposition rate in DMR conditions and will be discussed below. By increasing the temperature above 800 °C, reforming reactions are favored compared to carbon deposition (cf figure 1). For a typical SOFC operation temperature of above 800 °C with a CH_4 to CO_2 ratio higher than 1, the risk of carbon deposition is theoretically low.

Another strategy to mitigate carbon deposition is tailoring the CH_4 to CO_2 ratio in the feed gas, which is named $R = CH_4/CO_2$. Theoretically, an increase in the content of the dry reforming agent CO_2 leads to a reduced chance of carbon deposition (cf figure 1) [100]. However, in the literature, contradictory results are published by several working groups. In the case of simulated biogas with $R = 1.5$ at 800 °C and under a current load of 200 mA·cm^{-2}, no carbon deposition was observed for an operation of 800 h [101]. This is following another study that did not observe carbon deposition for an R-value as high as 1.7 at 800 °C and without current [102]. In contrast, another study found carbon deposition at 850 °C for an R above 1 and no carbon deposition for an R below 1 [47]. Even lower R values in the range of 0.5–0.75 have been suggested to prevent carbon deposition and ensure a stable operation [103]. This is in line with other studies which suggested R values of 0.55 and 0.67 [49, 104].

Another way to avoid carbon deposition is the injection of a small amount of steam into the feed gas. Theoretically, H_2O addition moves the operation conditions to the non-carbon deposition region as shown

in figure 1. The same result can be achieved by adding oxygen. However, here the risk of nickel reoxidation in the Ni-containing fuel electrode must be considered. Operating an SOFC with increased current density is another strategy to lessen carbon deposition. The oxygen atom concentration at the fuel electrode is increased which can shift the operation thermodynamically in the carbon deposition-free region. Furthermore, one study claimed that deposited carbon is hydrogenated and removed from the fuel electrode surface when applying high current densities [105]. In conclusion, the thermodynamics of carbon deposition in DMR are well described and understood in the literature. However, the kinetics are still not well evaluated. In addition, contradictory results are described in studies for the safe operation of an SOFC with DRM. Here the authors think that an insufficient description of the working parameters e.g. conversion rates, feed gas flow rates or residence, insufficient degradation times (under 1000 h) or insufficient post-test characterization must be addressed in the future. Furthermore, the effect of N_2 as a filling gas on the DRM reaction in SOFC should be evaluated.

Further strategies for preventing carbon deposition are also described in the literature. One approach is the verification or modification of the fuel electrode material. For instance, state-of-the-art Ni-YSZ and Ni-GDC fuel electrodes can be modified to vary the Ni properties. Catalyst promoters can be used in the form of a bi-metallic metal–Ni alloy with promoters such as Co, Cu, Sn, Pt, Pd, or other noble metals. Here, an increase in H_2 selectivity and a decrease in carbon deposition is favorable. A more detailed review of catalyst modification for methane reforming in SOFC has been already published [95]. The catalysts are evaluated in terms of performance and carbon resistance but not from a technical or economic point of view. Furthermore, often only separated processes are investigated and not the overall processes of DMR and SOFC operation combined.

The implementation of an additional internal reforming layer on top of the fuel electrode is another strategy to mitigate carbon deposition. The investigation of a 3 wt.% Ru–Al_2O_3 layer on top of the Ni-YSZ fuel electrode included only short-term degradation tests and missed a technical and economic evaluation [106]. A more detailed description of the implementation of internal reforming layers can be found in [95].

4.2.2. Sulfur poisoning

Sulfur poisoning is known to be a critical issue in SOC operation leading to decreased stability and degradation. The chemisorption mechanism is shown in equation (22) and is believed to be mainly responsible for low sulfur concentrations:

$$H_2S_{(g)} \rightarrow S_{(ads)} + H_{2(g)} \tag{22}$$

Interestingly, the adsorption of sulfur is site-specific, thus only part of the Ni reaction sites are blocked [107, 108]. This is used to explain the abrupt initial passivation and the later constant passivation seen in sulfur-poisoned cells [107–109]. The passivation and deactivation are found to decrease with a decrease in H_2S concentration in the feed gas, an increase in current density, and an increase in operating temperature [108, 110–112].

As previously mentioned, biogas is a promising feed gas for the DMR process in an SOFC system. Interestingly, the passivation of sulfur poisoning is slower during dry reforming compared to wet reforming conditions [113, 114]. Fortunately, sulfur passivation is reversible for the exposure of low H_2S concentrations in the feed gas [108, 109, 112]. However, at higher concentrations of H_2S and bulk sulfidation, permanent degradation is observed [115]. There are several options to handle sulfur poisoning. One option would be the development of new catalysts/fuel electrodes. However, compatibility with the electrochemical performance of an SOFC and the direct DMR must be considered especially for nickel-free electrode materials. Another option is the treatment of feed gas e.g. biogas in a gas cleaning unit (GCU) [116]. A detailed summary of the options for biogas cleaning can be found in [117].

4.2.3. Halogens and siloxanes

Other contaminants can be critical for the operation of an SOFC. Especially, for the direct utilization of biogas in an SOFC system, siloxanes and halogenated compounds can be present in the inlet gas [118]. In biogas, siloxane and halogen concentrations vary between 0.1 and 10 ppm, and thus like sulfur-containing gas, a GCU must be applied. The effect of halogens on the operation of an SOFC is still not well understood. For instance, in H_2 rich atmosphere chlorine compounds are believed to decompose to HCl. HCl contamination must be seen as critical for the operation of an SOFC as it is reported to lead to accelerated degradation, however, far less detrimental than H_2S [119, 120]. For now, it is believed that the effect of HCl on the cell's performance is reversible and a concentration of around 5000 ppb is required for an impact on the stability [119, 121]. Other halogens have not been investigated in literature until now.

In the case of siloxanes, the amount of 10 ppb already has an impact on the cells' degradation [121]. In general, Si poisoning is repeatedly reported in the literature and well understood in SOCs. Silica impurities in

the feed gas led to the passivation and degradation of the Ni-containing fuel electrode, e.g. an accumulation at the TPBs leads to the blocking of catalytic sites [122]. In the case of biogas application, siloxanes and organosilicon compounds with chemical formulas represented as $[SiO(CH_3)_2]_n$ or $[SiO/C_6H_5)_2]_n$ can be found in the feed gas [123]. One study reported that severe degradation was observed after 50 h of operation with 10 ppm decamethylcyclopentasiloxane in the humidified hydrogen feed gas [123]. The degradation is associated with SiO_2 formation in the fuel electrode structure. Again, a GCU that filters most of the contaminants out of the inlet gases is the most suitable solution.

5. Conclusions and future perspectives

As shown in this paper, the internal reforming of CH_4 and CO_2, which are abundant and inexpensive, in a fuel cell is a highly flexible and efficient one-step process to co-generate electrical power and valuable gaseous products such as H_2 and CO directly from biogas. The internal reforming reaction in fuel cells at elevated temperatures bypasses the Carnot limitation. Additionally, the high energy demand of endothermic reforming could be met by existing industrial plants, thereby increasing the process efficiency and economic feasibility. However, DRM directly in an SOFC or SPCFC system is a complicated process in several aspects. SPCFCs enable high cell efficiencies at intermediate operating temperatures of 400 °C–650 °C and therefore mitigate the technical hurdles of material aging observed in SOFCs. Nevertheless, the technology readiness level (∼4) of proton conducting cells is constrained due to the lack of experimentally well-defined operating conditions, missing long-term durability experiments (>3000 h), and missing stack-level testing. An additional hindrance to the implementation of DRM in SPCFC systems will be the operating conditions. At the typical operating temperatures for SPCFCs below 700 °C, several side reactions occur, which lead to the formation of the side product steam (400 °C–820 °C) and undesirable surface carbon deposition (below 700 °C). Therefore, the optimal operating conditions (temperature, pressure, feed gas) and poisoning-resistant materials (e.g. carbon) have to be investigated. Additional studies should focus on the improvement of the currently in-use SPCFC materials to improve catalytic activity, advance sulfur tolerance and increase carbon resistance at intermediate temperatures. Unlike most current studies, cell development will need to be taken to bench scale and include long-term durability testing over 1000 h as well as future research into cell models for SPCFCs.

SOFC systems are at a higher TRL (∼7–9) and already commercially available. The higher operating temperatures mitigate the formation of carbon or steam and shift the reaction equilibrium to the desired product mixture of CO and H_2. Higher temperatures are additionally favorable for the highly endothermic DMR reaction. The long-term operation of the SOFC system has been validated for hydrogen production over more than 100 000 h and meets targeted low degradation rates of $0.5\%{\cdot}kh^{-1}$. Future research has to be conducted into the feasibility of long-term DRM in SOFCs. The investigation of internal DRM has shown the possible combination of the reformer unit directly with an option to produce energy from H_2 within the SOFC and simultaneously tailoring the outlet gases is attractive, as investment and operating costs can be saved. Besides the possible beneficial utilization of CO_2 emissions, DRM is typically operated at 1 atm and around 850 °C and thus less energy-intensive than the established steam methane reforming process. SMR is operated at elevated pressures over 15 atm and temperatures up to 1000 °C [124]. As shown above, several studies have already demonstrated the feasibility of converting dry methane in an SOFC system. However, even study results on button cells have been contradictory regarding the optimal operation conditions e.g. to prevent carbon deposition during operation. Therefore, scaling up to the system level and understanding these conditions in terms of thermodynamics and kinetics is necessary to ensure safe operation over the years. For instance, the effects of power fluctuations, shutdown times, temperature distribution, and stability over years of other components of an SOFC system need to be considered in future work. Additionally, temperature distribution, gas conversion, and gas content homogeneity along the flow paths are complex parameters to balance in an SOFC systems. Another challenge to overcome is that cell optimization has been investigated for H_2 utilization but not the simultaneous reforming reaction. Here, detailed impedance spectroscopy and analysis of activation energies or processes by the distribution of relaxation times could help to distinguish both reactions and tailor the 'perfect' cell. Especially, the degradation mechanisms described above, and the challenges of temperature distribution of the endothermic reforming and the exothermic fuel cell operation must be considered. Studies that present solutions often do not discuss the economic or technical feasibility of, for example, new materials or the introduction of additional layers. Here, a direct DMR system incorporating an SOFC must prove to be better or comparable to existing alternative mature technologies in terms of economic, technological, and efficiency aspects.

Data availability statement

The data that support the findings of this study are available upon reasonable request from the authors.

Acknowledgment

The authors gratefully acknowledge funding provided by the German Federal Ministry of Education and Research (BMBF) within the SOC-Degradation 2.0 project: Transfer of knowledge into products for a 'green hydrogen' vector—Impedance analysis of intrinsic and extrinsic degradation mechanisms in SOC cells and repeat units (FKZ 03SF0621A) and the research project iNEW 2.0 'Incubator for Sustainable Electrochemical Value Chains' (FKZ: 03SF0627A).

ORCID iDs

Stephanie E Wolf https://orcid.org/0000-0002-9627-7121
Jan Uecker https://orcid.org/0000-0002-4261-4508
Niklas Eyckeler https://orcid.org/0000-0002-4703-3155
Leon Schley https://orcid.org/0009-0008-9920-1262
L G J (Bert) de Haart https://orcid.org/0000-0001-6908-1214
Vaibhav Vibhu https://orcid.org/0000-0001-9157-2722
Rüdiger-A Eichel https://orcid.org/0000-0002-0013-6325

References

[1] Peschel A 2020 Industrial perspective on hydrogen purification, compression, storage, and distribution *Fuel Cells* **20** 385–93
[2] IEA 2023 *Global Hydrogen Review 2023*
[3] Wolf S E, Winterhalder F E, Vibhu V, de Haart L G J, Guillon O, Eichel R-A and Menzler N H 2023 Solid oxide electrolysis cells—current material development and industrial application *J. Mater. Chem.* A **11** 17977–8028
[4] Ryckebosch E, Drouillon M and Vervaeren H 2011 Techniques for transformation of biogas to biomethane *Biomass Bioenergy* **35** 1633–45
[5] Sun Q, Li H, Yan J, Liu L, Yu Z and Yu X 2015 Selection of appropriate biogas upgrading technology-a review of biogas cleaning, upgrading and utilisation *Renew. Sustain. Energy Rev.* **51** 521–32
[6] Yang L, Ge X, Wan C, Yu F and Li Y 2014 Progress and perspectives in converting biogas to transportation fuels *Renew. Sustain. Energy Rev.* **40** 1133–52
[7] Foit S R, Vinke I C, de Haart L G J and Eichel R-A 2017 Power-to-Syngas: an enabling technology for the transition of the energy system? *Angew. Chem., Int. Ed.* **56** 5402–11
[8] AlHumaidan F S, Absi Halabi M, Rana M S and Vinoba M 2023 Blue hydrogen: current status and future technologies *Energy Convers. Manage.* **283** 116840
[9] Selmert V, Kretzschmar A, Kungl H, Tempel H and Eichel R-A 2024 Breakthrough analysis of the CO_2/CH_4 separation on electrospun carbon nanofibers *Adsorption* **30** 107–19
[10] Pakhare D, Shaw C, Haynes D, Shekhawat D and Spivey J 2013 Effect of reaction temperature on activity of Pt- and Ru-substituted lanthanum zirconate pyrochlores ($La_2Zr_2O_7$) for dry (CO_2) reforming of methane (DRM) *J. CO_2 Util.* **1** 37–42
[11] Bradford M C J and Vannice M A 1999 CO_2 reforming of CH_4 *Catal. Rev.* **41** 1–42
[12] Pakhare D and Spivey J 2014 A review of dry (CO_2) reforming of methane over noble metal catalysts *Chem. Soc. Rev.* **43** 7813–37
[13] Chein R Y, Chen Y C, Yu C T and Chung J N 2015 Thermodynamic analysis of dry reforming of CH_4 with CO_2 at high pressures *J. Nat. Gas Sci. Eng.* **26** 617–29
[14] Guczi L, Stefler G, Geszti O, Sajó I, Pászti Z, Tompos A and Schay Z 2010 Methane dry reforming with CO_2: a study on surface carbon species *Appl. Catal.* A **375** 236–46
[15] Charisiou N D, Siakavelas G, Tzounis L, Sebastian V, Monzon A, Baker M A, Hinder S J, Polychronopoulou K, Yentekakis I V and Goula M A 2018 An in depth investigation of deactivation through carbon formation during the biogas dry reforming reaction for Ni supported on modified with CeO_2 and La_2O_3 zirconia catalysts *Int. J. Hydrog. Energy* **43** 18955–76
[16] Goula M A, Charisiou N D, Siakavelas G, Tzounis L, Tsiaoussis I, Panagiotopoulou P, Goula G and Yentekakis I V 2017 Syngas production via the biogas dry reforming reaction over Ni supported on zirconia modified with CeO_2 or La_2O_3 catalysts *Int. J. Hydrog. Energy* **42** 13724–40
[17] Argyle M and Bartholomew C 2015 Heterogeneous catalyst deactivation and regeneration: a review *Catalysts* **5** 145–269
[18] Moulijn J, van Diepen A and Kapteijn F 2001 Catalyst deactivation: is it predictable? *Appl. Catal.* A **212** 3–16
[19] Carrara C, Múnera J, Lombardo E A and Cornaglia L M 2008 Kinetic and stability studies of Ru/La_2O_3 used in the dry reforming of methane *Top. Catal.* **51** 98–106
[20] Ferreira-Aparicio P, Márquez-Alvarez C, Rodríguez-Ramos I, Schuurman Y, Guerrero-Ruiz A and Mirodatos C 1999 A transient kinetic study of the carbon dioxide reforming of methane over supported Ru catalysts *J. Catal.* **184** 202–12
[21] Wu Z, Yang B, Miao S, Liu W, Xie J, Lee S, Pellin M J, Xiao D, Su D and Ma D 2019 Lattice strained Ni-Co alloy as a high-performance catalyst for catalytic dry reforming of methane *ACS Catal.* **9** 2693–700
[22] García-Diéguez M, Pieta I S, Herrera M C, Larrubia M A and Alemany L J 2011 RhNi nanocatalysts for the CO_2 and $CO^2+ H_2O$ reforming of methane *Catal. Today* **172** 136–42
[23] Dal Santo V, Gallo A, Naldoni A, Guidotti M and Psaro R 2012 Bimetallic heterogeneous catalysts for hydrogen production *Catal. Today* **197** 190–205
[24] Bian Z, Das S, Wai M H, Hongmanorom P and Kawi S 2017 A review on bimetallic nickel-based catalysts for CO_2 reforming of methane *ChemPhysChem* **18** 3117–34

[25] Tsiotsias A I, Charisiou N D, Yentekakis I V and Goula M A 2020 Bimetallic Ni-based catalysts for CO_2 methanation: a review *Nanomaterials* **11** 28
[26] Yentekakis I V, Panagiotopoulou P and Artemakis G 2021 A review of recent efforts to promote dry reforming of methane (DRM) to syngas production via bimetallic catalyst formulations *Appl. Catal.* B **296** 120210
[27] Winter M and Brodd R J 2004 What are batteries, fuel cells, and supercapacitors? *Chem. Rev.* **104** 4245–69
[28] Ebbesen S D, Graves C and Mogensen M 2009 Production of synthetic fuels by co-electrolysis of steam and carbon dioxide *Int. J. Green Energy* **6** 646–60
[29] Ebbesen S D, Knibbe R and Mogensen M 2012 Co-electrolysis of steam and carbon dioxide in solid oxide cells *J. Electrochem. Soc.* **159** F482–F9
[30] Wolf S E, Dittrich L, Nohl M, Duyster T, Vinke I C, Eichel R-A and de Haart L G J 2022 Boundary investigation of high-temperature co-electrolysis towards direct CO_2 electrolysis *J. Electrochem. Soc.* **169** 34531
[31] Foit S, Dittrich L, Duyster T, Vinke I, Eichel R-A and de Haart L G J 2020 Direct solid oxide electrolysis of carbon dioxide: analysis of performance and processes *Processes* **8** 1390
[32] Dittrich L, Nohl M, Jaekel E E, Foit S, de Haart L G J and Eichel R-A 2019 High-temperature co-electrolysis: a versatile method to sustainably produce tailored syngas compositions *J. Electrochem. Soc.* **166** F971–F5
[33] Selmert V, Kretzschmar A, Weinrich H, Tempel H, Kungl H and Eichel R-A 2022 CO_2/N_2 separation on highly selective carbon nanofibers investigated by dynamic gas adsorption *ChemSusChem* **15** e202200761
[34] Smith G P *et al GRI-MECH 3.0* (available at: http://combustion.berkeley.edu/gri-mech/version30/text30.html)
[35] Prado F, Armstrong T, Caneiro A and Manthiram A 2001 Structural stability and oxygen permeation properties of $Sr_{3-x}LaxFe_{2-y}CoyO_{7-\delta}$ ($0\leqslant x\leqslant 0.3$ and $0\leqslant y\leqslant 1.0$) *J. Electrochem. Soc.* **148** J7
[36] Baratov S, Filonova E, Ivanova A, Bilal Hanif M, Irshad M, Zubair Khan M, Motola M, Rauf S and Medvedev D 2024 Current and further trajectories in designing functional materials for solid oxide electrochemical cells: a review of other reviews *J. Energy Chem.* **94** 302–31
[37] Jiang S P 2019 Development of lanthanum strontium cobalt ferrite perovskite electrodes of solid oxide fuel cells—a review *Int. J. Hydrog. Energy* **44** 7448–93
[38] Cassidy M 2017 Trends in the processing and manufacture of solid oxide fuel cells *WIREs Energy Environ.* **6** e248
[39] Menzler N H, Tietz F, Uhlenbruck S, Buchkremer H P and Stöver D 2010 Materials and manufacturing technologies for solid oxide fuel cells *J. Mater. Sci.* **45** 3109–35
[40] Tian Y, Abhishek N, Yang C, Yang R, Choi S, Chi B, Pu J, Ling Y, Irvine J T and Kim G 2022 Progress and potential for symmetrical solid oxide electrolysis cells *Matter* **5** 482–514
[41] Jang I, Carneiro J S A, Crawford J O, Cho Y J, Parvin S, Gonzalez-Casamachin D A, Baltrusaitis J, Lively R P and Nikolla E 2024 Electrocatalysis in solid oxide fuel cells and electrolyzers *Chem. Rev.* **124** 8233–306
[42] Moarrefi S, Jacob M, Li C, Cai W and Fan L 2024 Internal dry reforming of methane in solid oxide fuel cells *Chem. Eng. J.* **489** 151281
[43] Alsaffar M A, Ayodele B V, Ali J M, Abdel Ghany M A, Mustapa S I and Cheng C K 2021 Kinetic modeling and reaction pathways for thermo-catalytic conversion of carbon dioxide and methane to hydrogen-rich syngas over alpha-alumina supported cobalt catalyst *Int. J. Hydrog. Energy* **46** 30871–81
[44] Moon D J and Ryu J W 2003 Electrocatalytic reforming of carbon dioxide by methane in SOFC system *Catal. Today* **87** 255–64
[45] Yamamoto K and Sakaguchi K 2022 Hydrogen reactivity factor and effects of oxygen on methane conversion rate by chemical equilibrium calculation *Int. J. Therm. Sci.* **15** 100186
[46] Chein R Y, Hsu W H and Yu C T 2017 Parametric study of catalytic dry reforming of methane for syngas production at elevated pressures *Int. J. Hydrog. Energy* **42** 14485–500
[47] Saadabadi S A, Illathukandy B and Aravind P V 2021 Direct internal methane reforming in biogas fuelled solid oxide fuel cell; the influence of operating parameters *Energy Sci. Eng.* **9** 1232–48
[48] Staniforth J and Ormerod R M 2002 *Catal. Lett.* **81** 19–23
[49] Lanzini A and Leone P 2010 Experimental investigation of direct internal reforming of biogas in solid oxide fuel cells *Int. J. Hydrog. Energy* **35** 2463–76
[50] Farhad S, Hamdullahpur F and Yoo Y 2010 Performance evaluation of different configurations of biogas-fuelled SOFC micro-CHP systems for residential applications *Int. J. Hydrog. Energy* **35** 3758–68
[51] Santarelli M, Quesito F, Novaresio V, Guerra C, Lanzini A and Beretta D 2013 Direct reforming of biogas on Ni-based SOFC anodes: modelling of heterogeneous reactions and validation with experiments *J. Power Sources* **242** 405–14
[52] Fan D, Liu F, Li J, Wei T, Ye Z, Wang Z, Hu X, Dong D, Wang H and Shao Z 2021 A microchannel reactor-integrated ceramic fuel cell with dual-coupling effect for efficient power and syngas co-generation from methane *Appl. Catal.* B **297** 120443
[53] Wolf S E, Vibhu V, Coll C L, Eyckeler N, Vinke I C, Eichel R-A and de Haart L G J 2023 Long-term stability of perovskite-based fuel electrode material Sr_2 Fe_{2-X} Mo_x $O_{6-\delta}$—GDC for enhanced high-temperature steam and CO_2 electrolysis *ECS Trans.* **111** 2119–30
[54] Kreuer K D 2003 Proton-conducting oxides *Annu. Rev. Mater. Res.* **33** 333–59
[55] Schley L, Vibhu V, Nohl L, Vinke I C, de Haart L G J and Eichel R-A 2024 A highly stable $Pr_2NiO_{4+\delta}$ oxygen electrode in electrolyte supported protonic ceramic electrolysis cells (PCECs) for hydrogen production with high faradaic efficiency *Energy Adv.* **3** 861–73
[56] Fop S 2021 Solid oxide proton conductors beyond perovskites *J. Mater. Chem.* A **9** 18836–56
[57] Duan C, Kee R, Zhu H, Sullivan N, Zhu L, Bian L, Jennings D and O'Hayre R 2019 Highly efficient reversible protonic ceramic electrochemical cells for power generation and fuel production *Nat. Energy* **4** 230–40
[58] Choi S, Kucharczyk C J, Liang Y, Zhang X, Takeuchi I, Ji H-I and Haile S M 2018 Exceptional power density and stability at intermediate temperatures in protonic ceramic fuel cells *Nat. Energy* **3** 202–10
[59] Duan C, Huang J, Sullivan N and O'Hayre R 2020 Proton-conducting oxides for energy conversion and storage *Appl. Phys. Rev.* **7** 011314
[60] Choi S, Davenport T C and Haile S M 2019 Protonic ceramic electrochemical cells for hydrogen production and electricity generation: exceptional reversibility, stability, and demonstrated faradaic efficiency *Energy Environ. Sci.* **12** 206–15
[61] An H, Lee H-W, Kim B-K, Son J-W, Yoon K J, Kim H, Shin D, Ji H-I and Lee J-H 2018 A 5×5 cm^2 protonic ceramic fuel cell with a power density of 1.3 W cm^{-2} at 600 °C *Nat. Energy* **3** 870–5
[62] Zhang W, Zhang X, Song Y and Wang G 2024 Recent progress on cathode materials for protonic ceramic fuel cells *Next Sustain.* **3** 100028

[63] Zhu H, Ricote S, Duan C, O'Hayre R P, Tsvetkov D S and Kee R J 2018 Defect Incorporation and transport within dense $BaZr_{0.8}Y_{0.2}O_{3-\delta}$ (BZY20) proton-conducting membranes *J. Electrochem. Soc.* **165** F581–F8

[64] Zhu H, Ricote S, Duan C, O'Hayre R P and Kee R J 2018 Defect chemistry and transport within dense $BaCe_{0.7}Zr_{0.1}Y_{0.1}Yb_{0.1}O_{3-\delta}$ (BCZYYb) proton-conducting membranes *J. Electrochem. Soc.* **165** F845–F53

[65] Sata N and Costa R 2024 Protonic ceramic electrochemical cells in a metal supported architecture: challenges, status and prospects *Prog. Energy* **6** 32002

[66] Duan C *et al* 2018 Highly durable, coking and sulfur tolerant, fuel-flexible protonic ceramic fuel cells *Nature* **557** 217–22

[67] Chen Y *et al* 2018 A robust fuel cell operated on nearly dry methane at 500 °C enabled by synergistic thermal catalysis and electrocatalysis *Nat. Energy* **3** 1042–50

[68] Hong K, Choi M, Bae Y, Min J, Lee J, Kim D, Bang S, Lee H-K, Lee W and Hong J 2023 Direct methane protonic ceramic fuel cells with self-assembled Ni-Rh bimetallic catalyst *Nat. Commun.* **14** 7485

[69] Wei T, Qiu P, Jia L, Tan Y, Yang X, Sun S, Chen F and Li J 2020 Power and carbon monoxide co-production by a proton-conducting solid oxide fuel cell with $La_{0.6}Sr_{0.2}Cr_{0.85}Ni_{0.15}O_{3-\delta}$ for on-cell dry reforming of CH 4 by CO 2 *J. Mater. Chem.* A **8** 9806–12

[70] Hua B, Yan N, Li M, Sun Y-F, Zhang Y-Q, Li J, Etsell T, Sarkar P and Luo J-L 2016 Anode-engineered protonic ceramic fuel cell with excellent performance and fuel compatibility *Adv. Mater.* **28** 8922–6

[71] De S, Zhang J, Luque R and Yan N 2016 Ni-based bimetallic heterogeneous catalysts for energy and environmental applications *Energy Environ. Sci.* **9** 3314–47

[72] Kim D, Kang J, Lee Y, Park N, Kim Y, Hong S and Moon D 2008 Steam reforming of n-hexadecane over noble metal-modified Ni-based catalysts *Catal. Today* **136** 228–34

[73] Strohm J, Zhang J and Song C 2006 Low-temperature steam reforming of jet fuel in the absence and presence of sulfur over Rh and Rh–Ni catalysts for fuel cells *J. Catal.* **238** 309–20

[74] Ferrandon M, Kropf A J and Krause T 2010 Bimetallic Ni-Rh catalysts with low amounts of Rh for the steam and autothermal reforming of n-butane for fuel cell applications☆ *Appl. Catal.* A **379** 121–8

[75] Meng X, Gong X, Yang N, Yin Y, Tan X and Ma Z-F 2014 Carbon-resistant Ni-YSZ/Cu–CeO_2-YSZ dual-layer hollow fiber anode for micro tubular solid oxide fuel cell *Int. J. Hydrog. Energy* **39** 3879–86

[76] Hua B, Li M, Zhang W, Pu J, Chi B and Jian L 2014 Methane on-cell reforming by alloys reduced from $Ni_{0.5}Cu_{0.5}Fe_2O_4$ for direct-hydrocarbon solid oxide fuel cells *J. Electrochem. Soc.* **161** F569–F75

[77] Hua B, Li M, Pu J, Chi B and Jian L 2014 $BaZr_{0.1}Ce_{0.7}Y_{0.1}Yb_{0.1}O_{3-\delta}$ enhanced coking-free on-cell reforming for direct-methane solid oxide fuel cells *J. Mater. Chem.* A **2** 12576

[78] Hua B, Li M, Chi B and Jian L 2014 Enhanced electrochemical performance and carbon deposition resistance of Ni–YSZ anode of solid oxide fuel cells by *in situ* formed Ni–MnO layer for CH_4 on-cell reforming *J. Mater. Chem.* A **2** 1150–8

[79] Xie K, Yan R and Liu X 2009 Stable $BaCe_{0.7}Ti_{0.1}Y_{0.2}O_{3-\delta}$ proton conductor for solid oxide fuel cells *J. Alloys Compd.* **479** L40–L42

[80] Xie K, Yan R, Xu X, Liu X and Meng G 2009 The chemical stability and conductivity of $BaCe_{0.9-x}Y_xNb_{0.1}O_{3-\sigma}$ proton-conductive electrolyte for SOFC *Mater. Res. Bull.* **44** 1474–80

[81] Bi L, Tao Z, Liu C, Sun W, Wang H and Liu W 2009 Fabrication and characterization of easily sintered and stable anode-supported proton-conducting membranes *J. Membr. Sci.* **336** 1–6

[82] Fang S, Brinkman K S and Chen F 2014 Hydrogen permeability and chemical stability of Ni–$BaZr_{0.1}Ce_{0.7}Y_{0.1}Yb_{0.1}O_{3-\delta}$ membrane in concentrated H_2O and CO_2 *J. Membr. Sci.* **467** 85–92

[83] Zuo C, Dorris S E, Balachandran U and Liu M 2006 Effect of Zr-doping on the chemical stability and hydrogen permeation of the Ni−$BaCe_{0.8}Y_{0.2}O_{3-\alpha}$ mixed protonic−electronic conductor *Chem. Mater.* **18** 4647–50

[84] Prasad D H, Ji H-I, Kim H-R, Son J-W, Kim B-K, Lee H-W and Lee J-H 2011 Effect of nickel nano-particle sintering on methane reforming activity of Ni-CGO cermet anodes for internal steam reforming SOFCs *Appl. Catal.* B **101** 531–9

[85] Khan M S, Miura Y, Fukuyama Y, Gao S and Zhu Z 2022 Methane internal steam reforming in solid oxide fuel cells at intermediate temperatures *Int. J. Hydrog. Energy* **47** 13969–79

[86] Lyu Z, Shi W and Han M 2018 Electrochemical characteristics and carbon tolerance of solid oxide fuel cells with direct internal dry reforming of methane *Appl. Energy* **228** 556–67

[87] Shao X, Budiman R A, Sato T, Yamaguchi M, Kawada T and Yashiro K 2024 Review of factors affecting the performance degradation of Ni-YSZ fuel electrodes in solid oxide electrolyzer cells *J. Power Sources* **609** 234651

[88] Shang Y, Smitshuysen A L, Yu M, Liu Y, Tong X, Jørgensen P S, Rorato L, Laurencin J and Chen M 2023 3D microstructural characterization of Ni/yttria-stabilized zirconia electrodes during long-term CO 2 electrolysis *J. Mater. Chem.* A **11** 12245–57

[89] Weber A 2002 Oxidation of H_2, CO and methane in SOFCs with Ni/YSZ-cermet anodes *Solid State Ion.* **152–153** 543–50

[90] Mogensen M B, Chen M, Frandsen H L, Graves C, Hauch A, Hendriksen P V, Jacobsen T, Jensen S H, Skafte T L and Sun X 2021 Ni migration in solid oxide cell electrodes: review and revised hypothesis *Fuel Cells* **21** 415–29

[91] Hauch A, Ebbesen S D, Jensen S H and Mogensen M 2008 Solid oxide electrolysis cells: microstructure and degradation of the Ni/Yttria-stabilized zirconia electrode *J. Electrochem. Soc.* **155** B1184

[92] Trini M, Hauch A, Angelis S D, Tong X, Hendriksen P V and Chen M 2020 Comparison of microstructural evolution of fuel electrodes in solid oxide fuel cells and electrolysis cells *J. Power Sources* **450** 227599

[93] Jiao Z, Shikazono N and Kasagi N 2012 Quantitative characterization of SOFC nickel-YSZ anode microstructure degradation based on focused-ion-beam 3D-reconstruction technique *J. Electrochem. Soc.* **159** B285–B91

[94] Jiao Z, Busso E P and Shikazono N 2020 Influence of polarization on the morphological changes of nickel in fuel electrodes of solid oxide cells *J. Electrochem. Soc.* **167** 24516

[95] Fan L, Li C, Aravind P V, Cai W, Han M and Brandon N 2022 Methane reforming in solid oxide fuel cells: challenges and strategies *J. Power Sources* **538** 231573

[96] Höber M, Königshofer B, Schröttner H, Fitzek H, Menzler N H, Hochenauer C and Subotić V 2023 Experimental identification of the impact of direct internal and external methane reforming on SOFC by detailed online monitoring and supporting measurements *J. Power Sources* **581** 233449

[97] Girona K, Laurencin J, Fouletier J and Lefebvre-Joud F 2012 Carbon deposition in CH_4/CO_2 operated SOFC: simulation and experimentation studies *J. Power Sources* **210** 381–91

[98] Vafaeenezhad S, Hanifi A R, Laguna-Bercero M A, Etsell T H and Sarkar P 2022 Microstructure and long-term stability of Ni–YSZ anode supported fuel cells: a review *Mater. Futures* **1** 42101

[99] Nouri F, Maghsoudy S and Habibzadeh S 2024 Dynamic insights of carbon management and performance enhancement approaches in biogas-fueled solid oxide fuel cells: a computational exploration *Int. J. Hydrog. Energy* **50** 1314–28

[100] Khazaal M H, Staniforth J Z, Alfatlawi Z A, Ormerod R M and Darton R J 2018 Enhanced methane reforming activity of a hydrothermally synthesized codoped perovskite catalyst *Energy Fuels* **32** 12826–32
[101] Shiratori Y, Ijichi T, Oshima T and Sasaki K 2010 Internal reforming SOFC running on biogas *Int. J. Hydrog. Energy* **35** 7905–12
[102] Goula G, Kiousis V, Nalbandian L and Yentekakis I 2006 Catalytic and electrocatalytic behavior of Ni-based cermet anodes under internal dry reforming of CH_4+CO_2 mixtures in SOFCs *Solid State Ion.* **177** 2119–23
[103] Guerra C, Lanzini A, Leone P, Santarelli M and Brandon N P 2014 Optimization of dry reforming of methane over Ni/YSZ anodes for solid oxide fuel cells *J. Power Sources* **245** 154–63
[104] Rostrup-Nielsen J R, Sehested J and Nørskov J K 2002 Hydrogen and synthesis gas by steam- and CO_2 reforming *Adv. Catal.* **47** 65–139
[105] Chen T, Wang W G, Miao H, Li T and Xu C 2011 Evaluation of carbon deposition behavior on the nickel/yttrium-stabilized zirconia anode-supported fuel cell fueled with simulated syngas *J. Power Sources* **196** 2461–8
[106] Wang W, Ran R and Shao Z 2011 Combustion-synthesized Ru–Al_2O_3 composites as anode catalyst layer of a solid oxide fuel cell operating on methane *Int. J. Hydrog. Energy* **36** 755–64
[107] Ebbesen S D and Mogensen M 2009 Electrolysis of carbon dioxide in solid oxide electrolysis cells *J. Power Sources* **193** 349–58
[108] Rasmussen J F and Hagen A 2009 The effect of H_2S on the performance of Ni–YSZ anodes in solid oxide fuel cells *J. Power Sources* **191** 534–41
[109] Zha S, Cheng Z and Liu M 2007 Sulfur poisoning and regeneration of Ni-based anodes in solid oxide fuel cells *J. Electrochem. Soc.* **154** B201
[110] Hansen J B 2008 Correlating sulfur poisoning of SOFC nickel anodes by a Temkin isotherm *Electrochem. Solid-State Lett.* **11** B178
[111] Cheng Z, Zha S and Liu M 2007 Influence of cell voltage and current on sulfur poisoning behavior of solid oxide fuel cells *J. Power Sources* **172** 688–93
[112] Matsuzaki Y 2000 The poisoning effect of sulfur-containing impurity gas on a SOFC anode: part I. Dependence on temperature, time, and impurity concentration *Solid State Ion.* **132** 261–9
[113] Jablonski W S, Villano S M and Dean A M 2015 A comparison of H_2S, SO_2, and COS poisoning on Ni/YSZ and Ni/K_2O-$CaAl_2O_4$ during methane steam and dry reforming *Appl. Catal.* A **502** 399–409
[114] Johnson G B, Hjalmarsson P, Norrman K, Ozkan U S and Hagen A 2016 Biogas catalytic reforming studies on nickel-based solid oxide fuel cell anodes *Fuel Cells* **16** 219–34
[115] Hanna J, Lee W Y, Shi Y and Ghoniem A F 2014 Fundamentals of electro- and thermochemistry in the anode of solid-oxide fuel cells with hydrocarbon and syngas fuels *Prog. Energy Combust. Sci.* **40** 74–111
[116] Ouweltjes J P, Aravind P V, Woudstra N and Rietveld G 2006 Biosyngas utilization in solid oxide fuel cells with Ni/GDC anodes *J. Fuel Cell Sci. Technol.* **3** 495–8
[117] Golmakani A, Ali Nabavi S, Wadi B and Manovic V 2022 Advances, challenges, and perspectives of biogas cleaning, upgrading, and utilisation *Fuel* **317** 123085
[118] Papurello D, Soukoulis C, Schuhfried E, Cappellin L, Gasperi F, Silvestri S, Santarelli M and Biasioli F 2012 Monitoring of volatile compound emissions during dry anaerobic digestion of the organic fraction of municipal solid waste by proton transfer reaction time-of-flight mass spectrometry *Bioresour. Technol.* **126** 254–65
[119] Trembly J P, Gemmen R S and Bayless D J 2007 The effect of coal syngas containing HCl on the performance of solid oxide fuel cells: investigations into the effect of operational temperature and HCl concentration *J. Power Sources* **169** 347–54
[120] Bao J, Krishnan G N, Jayaweera P, Perez-Mariano J and Sanjurjo A 2009 Effect of various coal contaminants on the performance of solid oxide fuel cells: part I. Accelerated testing *J. Power Sources* **193** 607–16
[121] Ruokomäki J Biogas criteria for SOFC (available at: www.vtt.fi/inf/pdf/tiedotteet/2009/T2496.pdf) (Accessed 29 October 2024)
[122] Hauch A, Jensen S H, Bilde-Sørensen J B and Mogensen M 2007 Silica segregation in the Ni/YSZ electrode *J. Electrochem. Soc.* **154** A619
[123] Haga K, Adachi S, Shiratori Y, Itoh K and Sasaki K 2008 Poisoning of SOFC anodes by various fuel impurities *Solid State Ion.* **179** 1427–31
[124] Jarvis S M and Samsatli S 2018 Technologies and infrastructures underpinning future CO_2 value chains: a comprehensive review and comparative analysis *Renew. Sustain. Energy Rev.* **85** 46–68